Dalton Transactions

RSC Publishing

PAPER

View Article Online
View Journal | View Issue

Cite this: *Dalton Trans.*, 2013, **42**, 12926

Reversible hydrogen desorption from $LiBH_4$ catalyzed by graphene supported Pt nanoparticles

Juan Xu,[a,b] Zhongqing Qi,[a,b] Jianyu Cao,[a] Rongrong Meng,[a] Xiaofang Gu,[a] Wenchang Wang[a] and Zhidong Chen*[a,b]

Received 9th April 2013,
Accepted 2nd May 2013

DOI: 10.1039/c3dt50933h

www.rsc.org/dalton

The thermally induced de-/rehydrogenation performance of the graphene supported Pt nanoparticles (Pt/G) doped $LiBH_4$ was greatly improved even at very low catalyst content due to a synergetic effect of Pt addition and nanoconfinement in graphene. For the 5 wt% Pt/G doped $LiBH_4$ sample, the onset hydrogen desorption temperature is about 140 °C lower than that of the pure $LiBH_4$. With increasing loading of the Pt/G catalysts in $LiBH_4$ samples, the onset dehydrogenation temperature and the two main desorption peaks from $LiBH_4$ were found to decrease while the hydrogen release amount increased. About 17.8 wt% can be released from the 50 wt% Pt/G doped $LiBH_4$ sample below 500 °C. Moreover, variation of the equilibrium pressure (350–450 °C) indicates that the dehydrogenation enthalpy is reduced from 74 kJ mol^{-1} H_2 for the pure $LiBH_4$ to *ca.* 48 kJ mol^{-1} H_2 for the 10 wt% Pt/G doped $LiBH_4$, showing improved thermodynamic properties. More importantly, a reversible capacity of *ca.* 8.1 wt% in the 30th de-/rehydrogenation cycle was achieved under 3 MPa H_2 at 400 °C for 10 h, indicating that the Pt/G catalysts play a crucial role in the improvement of the hydrogen uptake reversibility of $LiBH_4$ at lower temperature and pressure conditions. Especially, $LiBH_4$ was reformed and a new product, $Li_2B_{10}H_{10}$, was detected after the rehydrogenation process.

1. Introduction

One key issue for the development of sustainable hydrogen economy is to explore efficient, reversible, safe and cheap hydrogen storage materials.[1] In particular, complex hydrides ($LiBH_4$, $NaBH_4$, $Al_3Li_4(BH_4)_{13}$, $NaNH_2$, *etc.*),[2–5] alloys (La_2MgNi_9, Mg_3MnNi_2, $Mg_{0.9}Ti_{0.1}Ni$, $Mg_{0.9}Ti_{0.1}NiAl_{0.05}$, *etc.*),[6–8] metal hydrides (MgH_2, Mg_2NiH_4, Mg_2CoH_5, Mg_3MnH_7, *etc.*)[9,10] and carbon materials (graphene, carbon nanotube, mesoporous carbon, *etc.*)[11,12] have attracted considerable attention due to their high storage capacities.

$LiBH_4$ is presently considered as one of the most promising hydrogen storage materials for hydrogen-powered vehicles as it offers a high theoretical hydrogen storage density (18.5 wt% H_2). However, the pure $LiBH_4$ is so unfavorably stable that only a limited degree of hydrogen uptake was acquired even at 600 °C and 35 MPa H_2,[2] which limits its practical applications for on-board hydrogen storage. Therefore, considerable strategies such as the destabilization with various effective catalysts, confinement in nanoporous materials, and partial cation substitution have been adopted to make the de-/rehydrogenation reaction of $LiBH_4$ more reversible and capable of operation under mild conditions.[13]

Various additives have been utilized to thermodynamically destabilize $LiBH_4$, reduce the desorption enthalpy and enhance de-/rehydrogenation kinetics. Züttel *et al.* reported that the initial hydrogen desorption temperature was decreased from 400 to 240 °C and about 9 wt% of hydrogen can be released below 400 °C in the case that $LiBH_4$ was ball-milled with SiO_2 micro particles with a mass ratio of 1 : 3.[14] Pan *et al.* reported that *ca.* 6.3 wt% hydrogen can be released from the $LiBH_4$–0.25TiF_4 composite below 150 °C with dramatically improved kinetics.[15] It was found that the synergetic effect of LaH_3 and MgH_2 on $LiBH_4$ is more effective than MgH_2 or LaH_3 alone,[16] and *ca.* 8.0 wt% hydrogen can be reversibly stored in the 6$LiBH_4$–CaH_2–3MgH_2 composite below 400 °C.[17] As reported by Shim *et al.*, the dehydrogenation reaction enthalpy of the $LiBH_4$–YH_3 composite was reduced to 51 KJ mol^{-1} H_2.[18] Moreover, the catalytic effect of transition metals (Ni, Co, Ru, Mg, Fe, *etc.*),[19–23] metal halides ($CdCl_2$, $MnCl_2$, $CuCl_2$, CaHCl, NbF_5, *etc.*),[24–29] and metal oxides (TiO_2, CeO_2, SiO_2, Fe_2O_3, Al_2O_3, *etc.*)[30,31] on the hydrogen storage properties of $LiBH_4$ have been widely investigated. Although these catalyst additives can lower the dehydrogenation temperature, increase the dehydrogenation capacity, and improve the reversibility, the requisite weight percent of most catalysts is so high that usually lead to an unsatisfactory weight ratio of

[a]*Jiangsu Key Laboratory for Solar Cell Materials and Technology, School of Petrochemical Engineering, Changzhou University, Changzhou 213164, China. E-mail: zdchen.lab@gmail.com; Fax: +86-0519-86330239; Tel: +86-0519-86330239*
[b]*Qualtec Co. Ltd., Changzhou 213164, China*

hydrogen. Thus, one essential research object is the quest for the efficient and low levels of catalysts.

On the other hand, improved thermal decomposition behaviors were successfully achieved by confining $LiBH_4$ in porous carbon materials to avoid the agglomeration effect. As confirmed by Yu *et al.*, the initial hydrogen desorption temperature was lowered to 250 °C and about 3.8 wt% hydrogen was released from the ball-milled $LiBH_4$ and multiwalled carbon nanotube (MWCNT) composite.[32] Agresti *et al.* also reported that the dehydrogenation temperature of $LiBH_4$ was decreased by more than 60 °C when $LiBH_4$ was dispersed on MWCNT by a solvent infiltration method.[33] About 7.5 wt% hydrogen was generated by the hydrolysis of the MWCNT doped $LiBH_4$.[34] In the meantime, other carbon catalysts like single-walled carbon nanotubes,[35] mesoporous carbon,[36–38] highly ordered hexagonal nanoporous hard carbon,[39] carbon aerogel,[40,41] carbon fibers[42] and fullerenes (C60)[43] were respectively used as substrates for $LiBH_4$, and various destabilized hydrogen storage systems were generated. Specifically, we found that the graphene catalysts doped $LiBH_4$ showed superior dehydrogenation and rehydrogenation performances to Vulcan XC-72, carbon nanotube and BP2000 doped $LiBH_4$.[44] Nevertheless, carbon catalysts with a high doping amount often results in the formation of inert fractions in the dehydrogenated sample. Nearly or even more than 50 wt% capacity loss in the first de-/rehydrogenation cycle was repeatedly observed in the high levels of carbon doped $LiBH_4$ samples.[32,33,36,37,44]

Recently, it was found that the dehydrogenation performance of $LiBH_4$ can be greatly improved by introducing both metallic catalysts and porous carbon materials. For example, Jongh *et al.* reported that the dehydrogenation temperature was decreased to *ca.* 350 °C,[45] and about 14 wt% of hydrogen can be absorbed at 320 °C under 4 MPa H_2 [19] because of the synergetic effects of Ni addition and nanoconfinement of nanoporous carbon. Mao *et al.* also reported that MWCNTs supported Ru nanoparticles can reduce the onset dehydrogenation temperature of the mixture of $LiBH_4$ and MgH_2 to 344 °C.[21] In our previous investigation we also found that the hydrogen release properties of the $LiBH_4$ doped with commercial carbon-supported Pt nanoparticles (Pt/C) can be improved significantly.[46] Despite these progresses, a huge challenge still remains to achieve reversible hydrogen uptake at moderate conditions and high hydrogen capacity simultaneously. Herein we investigate the hydrogen release and uptake processes of the as-milled graphene-supported Pt nanoparticles (Pt/G) doped $LiBH_4$ sample, as graphene possess huge surface area to uniformly disperse Pt NPs, and suitable pore size to confine $LiBH_4$ system.

2. Experimental section

2.1. Materials

Commercial $LiBH_4$ (95% purity, J&K Chemical Ltd, Sweden), natural graphite (99.9995% purity, Alfa Aesar Ltd, UK), $Na_2PtCl_6{\cdot}6H_2O$ (Alfa Aesar Ltd, UK), $NaNO_3$ (99% purity, Sinopharm Chemical Reagent Co. Ltd, China), $KMnO_4$ (99% purity, Sinopharm Chemical Reagent Co. Ltd, China), H_2SO_4 (96% purity, Sinopharm Chemical Reagent Co. Ltd, China), H_2O_2 (30% aqueous solution, Sinopharm Chemical Reagent Co. Ltd, China), carbon supported Pt nanoparticles (Pt/C, with a Pt loading of 60 wt%, HispecTM 9000, Johnson Matthey Inc., UK), platinum black (Pt, with surface area 28 $m^2\ g^{-1}$, Johnson Matthey Inc., UK), and polyvinyl pyrrolidone (PVP, Sinopharm Chemical Reagent Co. Ltd, China) were used as received.

2.2. Preparation of graphene oxide (GO)

GO used in present study was prepared by a complete oxidation and microwave irradiation method.[47] First, 1 g natural graphite powder was mixed with 1 g $NaNO_3$ in a reaction vessel that was preliminarily immersed in an ice bath and then, 35 mL H_2SO_4 was slowly added under violent stirring. In order to fully oxidize graphite powder to GO, 5 g $KMnO_4$ was gradually added into the above mixture over about 1 h at room temperature. Subsequently, the GO sample was added into a 100 mL 5 wt% H_2SO_4 aqueous solution over about 2 h with gentle stirring, and then 100 mL 30 wt% H_2O_2 was added. After centrifugation and washing with a mixed aqueous solution of 3 wt% H_2SO_4 and 0.5 wt% H_2O_2, the GO powder obtained was irradiated for 1 min in a domestic microwave oven (1100 W) and then was filtrated, washed and dried at 65 °C for 24 h.

2.3. Synthesis of Pt/G catalysts

Pt/G catalysts were prepared by an ethylene glycol (EG) co-reduction method under flowing argon. First of all, 200 mg GO was dispersed in a 400 mL 0.5 wt% PVP solution and exfoliated into single-layered GO sheets by ultrasonication (JAC 4020, 400 W, Sonic) for 100 min. After being filtered, rinsed with EG and dried at 50 °C, 100 mg GO was uniformly dispersed in a 100 mL EG solution. Meanwhile, 1.2 mL 0.0962 M Na_2PtCl_6, 2.1 mL 0.1 M EDTA, and 8 mL water were blended together, and kept at 60 °C for 40 min under vigorous stirring to form a bright yellow Pt-EDTA complex. After cooling the Pt-EDTA solution to room temperature, the above 1 mg mL^{-1} GO suspension was dropwise added under uniformly stirring for 4 h. Subsequently, a solution of 3.0 M NaOH in EG was added to adjust the pH value to above 13, and then the mixture was heated at 120 °C for 8 h to reduce the Pt and GO completely. After filtration, washing and drying under vacuum at 70 °C for 8 h, the Pt/G catalyst with a 60 wt% Pt loading was obtained. The filtrated solvent was colorless and the weight calculation based on thermogravimetric analysis showed that the Pt loading amount in the Pt/G catalyst is nearly 60 wt% during the deposition process.

2.4. Doping $LiBH_4$ with Pt/G catalysts

The mixture of $LiBH_4$ and Pt/G catalyst was prepared through a ball milling method: 1 g $LiBH_4$ and Pt/G mixture with various mass ratios was mechanically milled for 1.5 h (Planetary QM-1SP2) under argon atmosphere at room temperature. The ball-to-power weight ratio was 30 : 1 at 580 rpm using stainless

steel balls with 10 mm diameter. According to the same preparation process, pure graphene or Pt nanoparticles doped $LiBH_4$ was obtained. All the sample preparation was performed in the glove box under argon atmosphere to minimize H_2O and O_2 contamination.

2.5. Hydrogen releasing property measurements

In order to compare with the neat $LiBH_4$ system, the hydrogen capacity of the Pt/G doped $LiBH_4$ sample is calculated based only on the mass of pure $LiBH_4$ if it was not specifically pointed out, and the amount of impurities and added catalysts has been deducted.

Hydrogen desorption performance was investigated using a Netzsch STA449C TG-DSC thermoanalyzer coupled with a Balzers Thermostar Quadrupole Mass Spectrometer. Samples were heated at a rate of 10 °C min^{-1} under argon flowing at a purging rate of 20 cm^3 min^{-1}.

Cyclic hydrogen releasing properties were examined by volumetric method using a carefully calibrated Sievert's type apparatus. Typically, the 10 wt% Pt/G doped LBH_4 sample was repeatedly dehydrogenated at 550 °C for 5 h, and rehydrogenated at 400 °C with an initial 3 MPa hydrogen pressure for 10 h. As it is difficult to accurately characterize the rehydrogenation process under high hydrogen pressure, the restored hydrogen amounts were precisely determined in the subsequent dehydrogenation half-cycle.

2.6. Structure and morphology characterization

The morphology of the Pt/G catalysts was analyzed by transmission electron microscopy (TEM) using a Technai G2 20s-Twin Microscope (FEP Inc., USA). Samples were prepared by dispersing the dry Pt/G powder in ethanol to form a homogeneous suspension, and then dropped on a 300-mesh copper grid for observation.

X-ray diffraction (XRD) measurements were carried out to investigate the structure change and infer the possible reaction mechanism during the de-/rehydrogenation process. Diffraction patterns were collected on a Rigaku D/MAX-2500 diffractometer with Cu Kα radiation at a scanning rate of 2° min^{-1} and with a step of 0.02°.

3. Results and discussion

3.1. Microstructure characterization of the Pt/G catalysts

Fig. 1 presents TEM image of the Pt/G catalyst as well as its corresponding particle size distribution histogram. As observed, highly dispersed Pt nanoparticles with a relatively narrow particle size distribution are uniformly attached to large, disordered and over-lapped multilayer graphene sheets by a simple and cost-effective procedure. No aggregated Pt nanoparticles were observed, showing that graphene can stabilize the Pt nanoparticles and prevent them from aggregation. The mean size of the Pt nanoparticles on graphene support is *ca.* 4.1 nm, which was obtained by measuring more than 200 nanoparticles randomly.

3.2. Dehydrogenation properties of the Pt/G catalyst doped $LiBH_4$

Fig. 2 presents temperature programmed hydrogen release profiles and corresponding thermogravimetric (TG) curves of $LiBH_4$ doped with the Pt/G catalyst at different doped amounts, while the detailed data are listed in Table 1. The pure $LiBH_4$ requires a temperature of *ca.* 420 °C to desorb main hydrogen and reaches two peaks at 485 and 610 °C. The total weight loss is 10.7 wt% (curve a), indicating that only half of the hydrogen was released from the pure $LiBH_4$. However, even by adding 5 wt% of the Pt/G catalyst to the $LiBH_4$ compound, the onset hydrogen desorption temperature of $LiBH_4$ still shifts to 280 °C, about 140 °C lower than that of the pure $LiBH_4$ milled for an identical period, and the other main dehydrogenation peaks of the Pt/G doped $LiBH_4$ locates at 340 and 525 °C, with an increased total weight loss of 12.6 wt% (curve b). With increase in the Pt/G content, the onset dehydrogenation temperature and two main desorption peaks from the mixtures of Pt/G and $LiBH_4$ (up to 50 wt%), are gradually decreased while the total hydrogen release amount was found to increase. When $LiBH_4$ is doped with 50 wt% Pt/G, the onset dehydrogenation temperature approaches 150 °C, and the two major desorption peaks occur at 200 and 330 °C (curve e in Fig. 2(A)). Importantly, the dehydrogenation capacity of the 50 wt% Pt/G catalyst doped $LiBH_4$ is 17.8 wt% (curve e in Fig. 2

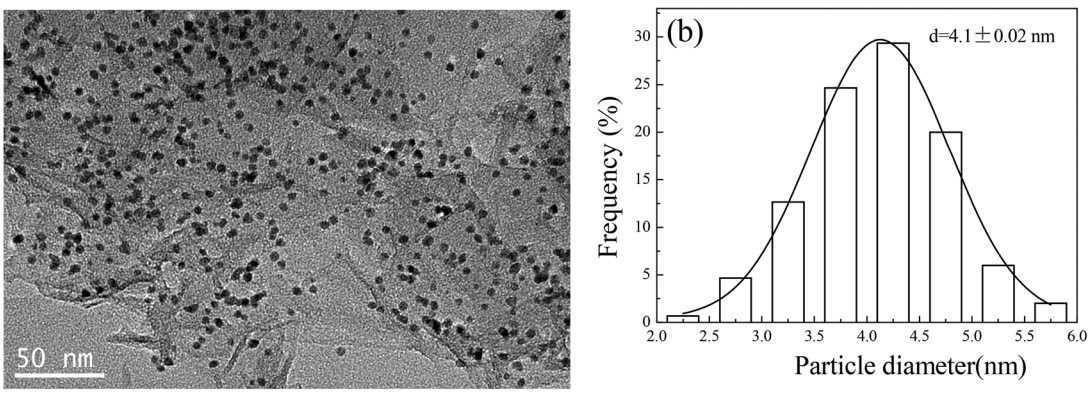

Fig. 1 TEM image (a) and corresponding particle size distribution histogram (b) of the Pt/G catalyst.

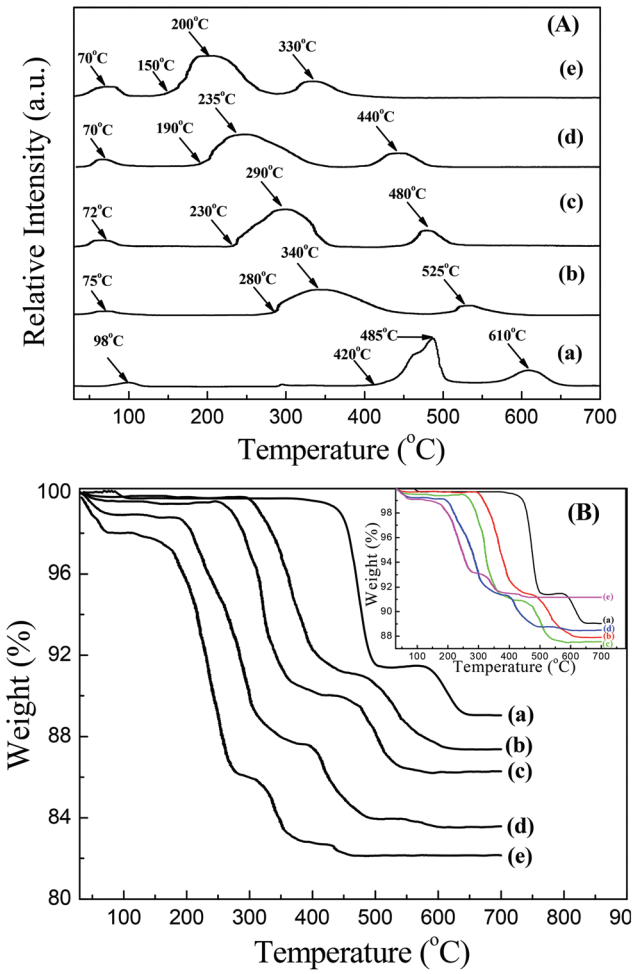

Fig. 2 Temperature programmed hydrogen release profiles (A) and TG curves (B) based on pure $LiBH_4$ for the evolution of hydrogen from the mixture of Pt/G and $LiBH_4$. The weight percentages of as-prepared Pt/G in the mixture of Pt/G and $LiBH_4$ are 0 (a), 5 wt% (b), 10 wt% (c), 30 wt% (d) and 50 wt% (e), respectively. The inset shows the real H_2 wt% based on the total amount of Pt/G catalysts and $LiBH_4$.

Table 1 Hydrogen release properties of the mixtures of Pt/G-60 and $LiBH_4$ with various mass ratios

Sample	Pt/G weight (wt%)	Onset T_{desorb}[a] (°C)	Main T_{desorb}[a] (°C)	H_2 desorbed (wt%)
$LiBH_4$	0	420	485; 610	10.7
Doped $LiBH_4$	5	280	340; 525	12.6
Doped $LiBH_4$	10	230	290; 480	13.7
Doped $LiBH_4$	30	190	235; 440	16.4
Doped $LiBH_4$	50	150	200; 330	17.8

[a] T_{desorb} represents the desorption temperature.

(B)), which is very close to the theoretical value of *ca.* 18.5 wt%. The onset dehydrogenation temperature is greatly decreased and the quantity of hydrogen desorbed from $LiBH_4$ is highly increased even using the Pt/G catalyst with a very low content.

The real hydrogen release amount based on the total amount of both the Pt/G catalysts and $LiBH_4$ is shown in the inset of Fig. 2(B). Compared with the weight loss of 10.7 wt% for the pure $LiBH_4$ (curve a), the real dehydrogenation capacity of the 5 wt%, 10 wt% and 30 wt% Pt/G doped $LiBH_4$ sample reaches 12.1, 12.5 and 11.5 wt% (curve b–d), respectively. On the other hand, the real hydrogen release amount from the 50 wt% Pt/G doped $LiBH_4$ sample is only 8.9 wt% (curve e), less than that of the pure $LiBH_4$, indicating that the overhigh doping amount can lead to an unsatisfactory weight ratio of hydrogen.

Fig. 3 shows B_2H_6 release of the pure $LiBH_4$, 10 wt% graphene and Pt/G doped $LiBH_4$. Compared with the pure $LiBH_4$, no B_2H_6 gas was detected from the MS profile of the Pt/G or graphene doped $LiBH_4$ during the heating process up to 550 °C, which may come from the micro-mesopores structure of graphene, in good agreement with the data of $LiBH_4$ doped by titanate nanotube and carbon templates.[48,49] These results clearly demonstrate that the total weight loss of the Pt/G doped $LiBH_4$ is solely attributed to the hydrogen release.

In order to elucidate the possible roles of graphene and Pt nanoparticles in the catalytical dehydrogenation of $LiBH_4$, a comparison of dehydrogenation behaviors of $LiBH_4$ doped with graphene, pure Pt nanoparticles and Pt/G catalysts at 50 wt% doping amount is determined in Fig. 4. In the case of $LiBH_4$ doped with the pure graphene catalyst, the first dehydrogenation temperature for the $LiBH_4$ sample starts at *ca.* 210 °C, and the temperatures for two major desorption peaks are 290 and 465 °C, with a hydrogen released amount of 12.8 wt% (curve a), demonstrating better hydrogen release properties than the pure $LiBH_4$. For the $LiBH_4$ doped with pure Pt nanoparticles, the first dehydrogenation temperature locates at *ca.* 305 °C, two main hydrogen desorption peaks occur at 375 and 590 °C, and 15.4 wt% hydrogen can be released (curve b). By adding the Pt/G catalyst to $LiBH_4$, the initial dehydrogenation temperature of $LiBH_4$ transfers to 150 °C, and the main dehydrogenation peaks of $LiBH_4$ shift to 200 and 330 °C, with an greatly increased weight loss of 17.8 wt% (curve c). In

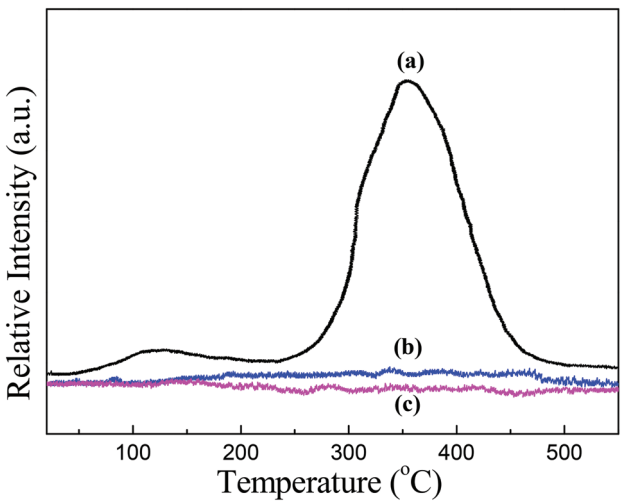

Fig. 3 B_2H_6 release with increasing temperature for the pure $LiBH_4$ (a), graphene (b) and Pt/G (c) doped $LiBH_4$. The loading amount of catalysts is 10 wt%.

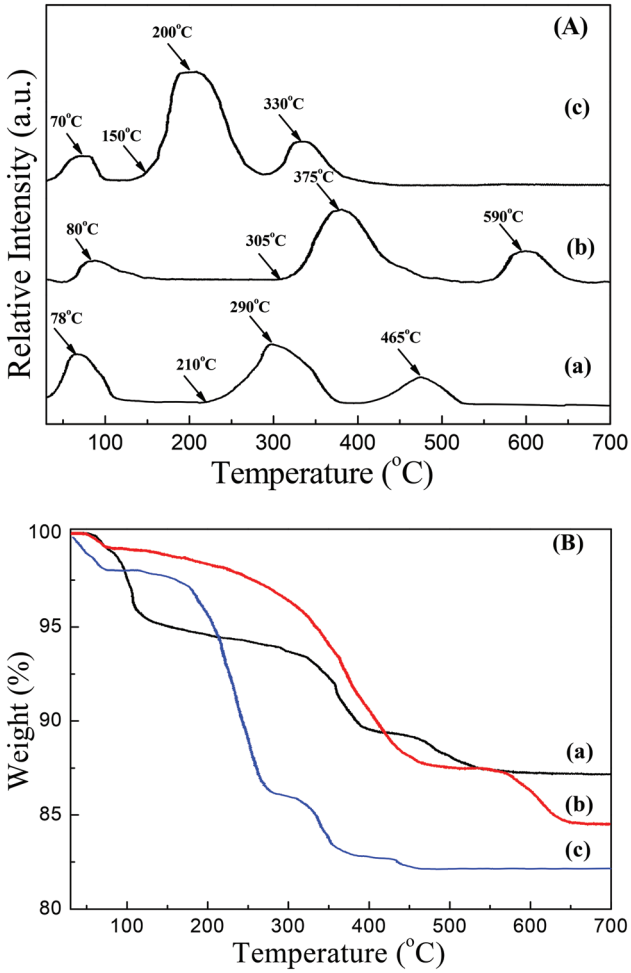

Fig. 4 Temperature programmed hydrogen release profiles (A) and TG curves (B) of the pure graphene (a), pure Pt nanoparticles (b) and Pt/G (c) catalysts doped $LiBH_4$. The doping amount of various catalysts is 50 wt%.

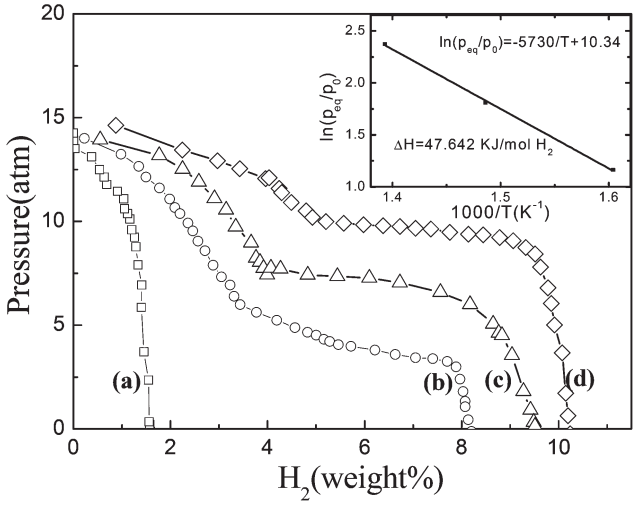

Fig. 5 Desorption PCT curves for pure $LiBH_4$ at 400 °C (a), 10 wt% Pt/G doped $LiBH_4$ at 350 (b), 400 (c), and 450 °C (d), respectively. The inset shows the van't Hoff plot for the dehydrogenated Pt/G doped $LiBH_4$ sample.

comparison to the pure $LiBH_4$, the dehydrogenation of the graphene or Pt nanoparticles doped $LiBH_4$ shifts to lower temperature and larger amount of hydrogen can be released, suggesting that both graphene and Pt nanoparticles can dramatically destabilize $LiBH_4$. Furthermore, the Pt/G catalysts present significantly higher catalytic effect on $LiBH_4$ than graphene and Pt nanoparticles alone, proving that the observed catalytic enhancement of $LiBH_4$ is the combined effect of graphene and Pt nanoparticles. The remarkable improvement in dehydrogenation properties is likely attributable to increased contact area between Pt/G catalyst and $LiBH_4$, newly produced structure defects during the ball-milling process for forming the composite material, and nanoconfinement effect of $LiBH_4$ in graphene.

After the hydrogen desorption performances of the Pt/G doped $LiBH_4$ sample have been ascertained, its dehydrogenation pressure-composition isotherms were collected to further investigate its thermodynamic properties and dehydrogenation behavior. Pressure–composition–temperature (PCT) measurements on the ball-milled pure $LiBH_4$ and 10 wt% Pt/G doped $LiBH_4$ were conducted in the range of 350–450 °C, as shown in Fig. 5. No plateaus can be observed for the pure $LiBH_4$ sample measured at 400 °C (curve a), while the dehydrogenation isotherms of the 10 wt% Pt/G doped $LiBH_4$ show obvious plateaus (curves b–d). As for the dehydrogenation at 450 °C, the dehydrogenation plateau was kept from 4.7 to 9.3 wt% and the total hydrogen capacity is approximately 10.3 wt% (curve d).

The van't Hoff plot for the dehydrogenation reaction of the 10 wt% Pt/G doped $LiBH_4$ system (logarithm of the equilibrium pressure *versus* the inverse of the absolute temperature), using the medium equilibrium pressures, is shown in the inset of Fig. 5. According to van't Hoff equation and the determined thermodynamic parameters, the resultant van't Hoff equation of the 10 wt% Pt/G doped $LiBH_4$ sample can be numerically expressed as $\ln(p_{eq.}/p_0) = -5730/T + 10.34$, and the dehydrogenation reaction enthalpy changes (ΔH) are calculated as *ca.* 48 kJ mol^{-1} H_2, which is far less than that of pure $LiBH_4$ (*ca.* 74 kJ mol^{-1} H_2),[33,50] demonstrating that the dehydrogenation thermodynamics of $LiBH_4$ is largely improved through the doping of Pt/G catalysts. It may due to the nanoconfinement effect of $LiBH_4$ within porous graphene scaffold hosts.[51–53]

3.3. Rehydrogenation properties of the Pt/G doped $LiBH_4$

The theoretical reversible hydrogen storage of the pure $LiBH_4$ below 600 °C is governed by the equilibrium, $LiBH_4 \rightleftharpoons LiH + B + 1.5H_2$, which accounts for a reversible hydrogen capacity of 13.9 wt%. However, the rehydrogenation condition is rather demanding due to slow kinetics, which leads to serious cyclic capacity degradation. In order to develop a reversible H_2 storage and release system for practical applications, the 10 wt% Pt/G doped $LiBH_4$ sample that had been dehydrogenated for 5 h under a vacuum up to 550 °C were rehydrogenated at 400 °C for 10 h under 3 MPa hydrogen pressure. Fig. 6 presents a comparison on cycling

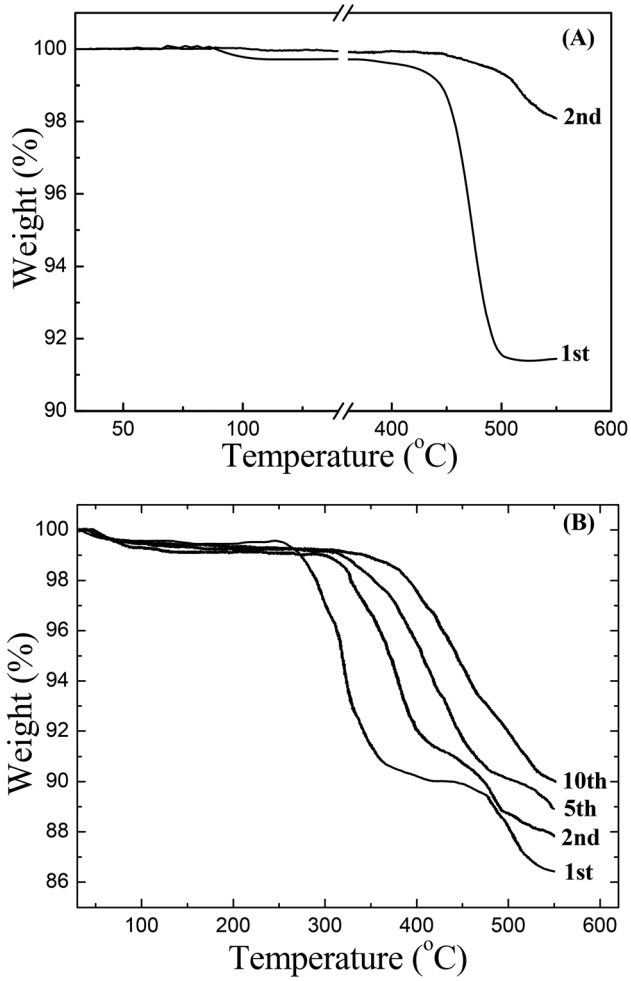

Fig. 6 Comparison on the dehydrogenation cycle profiles between the pure LBH_4 (A) and 10 wt% Pt/G doped LBH_4 (B). The Pt/G catalyst doped LBH_4 sample can be dehydrogenated (at 550 °C for 5 h) and rehydrogenated (at 3 MPa H_2, 400 °C for 10 h) repeatedly and measured gravimetrically.

dehydrogenation properties between the neat $LiBH_4$ and 10 wt% Pt/G doped $LiBH_4$ after recombination with H_2. Clearly, for the pure $LiBH_4$ sample, only 2.1 wt% hydrogen could be restored within 10 h at 400 °C with an initial hydrogen pressure of 3 MPa after the first rehydrogenation (Fig. 6 (A)). In contrast, the total H_2 released amount of the 10 wt% Pt/G doped $LiBH_4$ sample decreases from the initial 13.7 wt% to the 12.2 wt% in the second cycle, and further to 11.0 wt% in the fifth cycle and to 9.9 wt% in the tenth cycle (Fig. 6(B)). These results indicate that the cyclic capacity and capacity retention of the 10 wt% Pt/G doped $LiBH_4$ sample is much higher than that of pure $LiBH_4$.

Fig. 7 shows cyclic capacity life of the 10 wt% Pt/G and graphene doped $LiBH_4$, respectively. The capacity of the Pt/G doped $LiBH_4$ sample at the 30th cycles is still kept at *ca.* 8.1 wt%, while that of the graphene doped $LiBH_4$ sample at the tenth dehydrogenation is only 3.2 wt% H_2, indicating that Pt nanoparticles can greatly improve the hydrogen release and uptake reversibility of $LiBH_4$. Although it is still

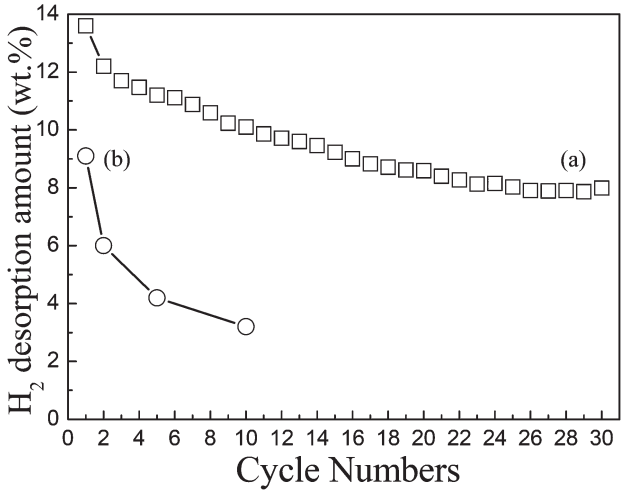

Fig. 7 Comparison on cycle life of the 10 wt% Pt/G (a) and graphene (b) doped $LiBH_4$.

somewhat lower than the 2015 hydrogen storage target set by the DOE system: 9 wt% H_2, the reversible hydrogen amount is much higher than those reported in literatures,[18,46,54,55] and substantially lower temperature and pressure conditions were applied.

In order to clarify the possible role of graphene substrate in the rehydrogenation process, TG curves of the 10 wt% Pt/G or commercial Pt/C doped $LiBH_4$ for the first and fourth dehydrogenation are determined in Fig. 8. The dehydrogenation capacities of the Pt/G or Pt/C doped $LiBH_4$ at the first dehydrogenation are 13.7 wt% and 13.1 wt%, respectively. For the fourth dehydrogenation, the weight loss corresponds to 11.2 wt% for the Pt/G doped $LiBH_4$ (curve c), but only 5.3 wt% for the commercial Pt/C doped $LiBH_4$ (curve d). These results proved that the cyclic reversibility of $LiBH_4$ was much better when the graphene substrate exists, which maybe due to that

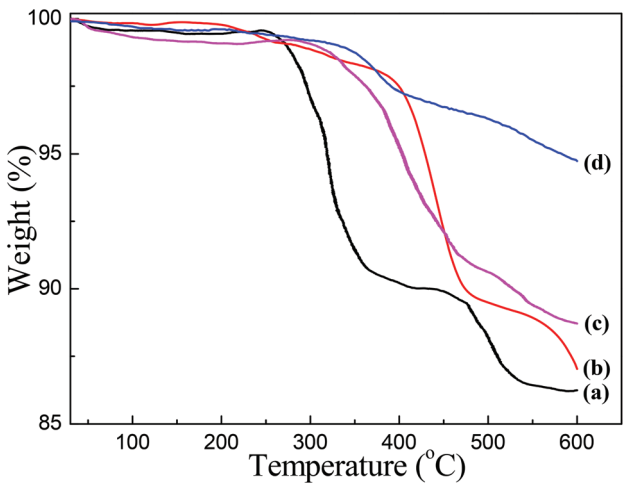

Fig. 8 TG profiles for the 10 wt% Pt/G (a, c) and commercial Pt/C (b, d) doped $LiBH_4$ at the first (a, b) and the fourth dehydrogenation (c, d) after recharging H_2.

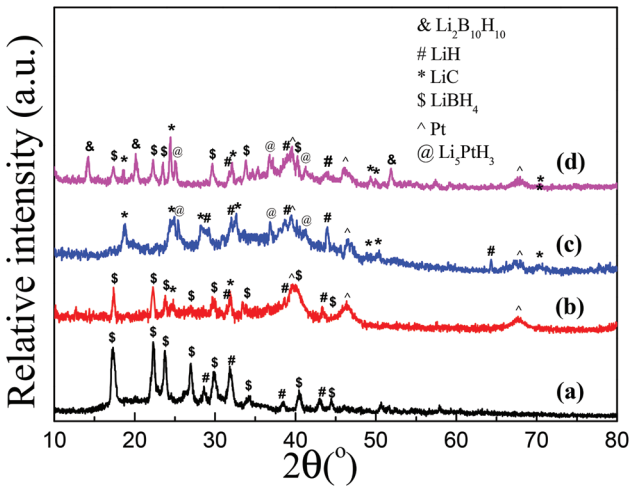

Fig. 9 XRD patterns for the ball-milled pure $LiBH_4$ (a), 10 wt% Pt/G doped $LiBH_4$ before (b) and after (c) the first dehydrogenation at 550 °C for 5 h, and after the tenth rehydrogenation (d) at 400 °C for 10 h with an initial hydrogen pressure of 3 MPa.

graphene possess huge surface area to uniformly disperse Pt nanoparticles.

3.4. Dehydrogenation/rehydrogenation reaction mechanism

To elucidate the possible reaction mechanism during the re-/dehydrogenation process and investigate the kinetic enhancement arising upon adding the Pt/G catalysts, Fig. 9 shows XRD patterns of the ball-milled pure $LiBH_4$, 10 wt% Pt/G doped $LiBH_4$ in the as-milled status, initial dehydrogenation condition at 550 °C for 5 h, and the tenth rehydrogenation state at 400 °C for 10 h. For the ball-milled pure $LiBH_4$, only $LiBH_4$ and LiH diffraction peaks are observed (curve a); the minor appearance of the LiH peaks may result from slight decomposition of $LiBH_4$ during the ball milling process. After the doping of Pt/G catalysts, new Pt and LiC diffraction peaks appears besides the $LiBH_4$ and LiH (curve b), indicating that the Pt/G catalyst can react with $LiBH_4$ to form LiC. The decomposition product of B from $LiBH_4$ is suggested to be amorphous state by ^{11}B NMR results in literatures,[55,56] and therefore, cannot be detected by XRD. After the first dehydrogenation at 550 °C for 5 h, the $LiBH_4$ phase disappears, and Pt, LiC, LiH and Li_5PtH_3 phases are identified (curve c). The possible dehydrogenation reaction may be described as $LiBH_4 \rightarrow LiH + B + 1.5H_2$, $LiBH_4 + C \rightarrow LiC + B + 2H_2$ and $5LiH + Pt \rightarrow Li_5PtH_3 + H_2$, catalyzed by the Pt/G catalyst. In the case of the rehydrogenated sample, $LiBH_4$ is reformed and one new product, $Li_2B_{10}H_{10}$, is detected (curve d), confirming the reversible dehydrogenation and rehydrogenation reactions of the Pt/G doped $LiBH_4$ sample. Nevertheless, LiC, LiH and Li_5PtH_3 phases still exist, showing incomplete rehydrogenation reaction, which may be the reason for the cyclic hydrogen capacity degradation of the Pt/G doped $LiBH_4$ sample. Thus, it was deduced that the reversible hydrogen uptake and release of the Pt/G doped $LiBH_4$ samples may be represented as follows: $LiH + B + 1.5H_2 \rightleftharpoons LiBH_4$ and $2LiH + 10B + 4H_2 \rightleftharpoons Li_2B_{10}H_{10}$.

4. Conclusions

The de-/rehydrogenation performances, reversibility and kinetics of $LiBH_4$ were markedly enhanced upon mechanically milling with the Pt/G catalysts even at extremely low catalyst content due to the combined effect of graphene and Pt nanoparticles, and the graphene supported Pt nanoparticles presents significantly higher catalytic effect on $LiBH_4$ than pure graphene or Pt nanoparticles alone. Moreover, the dehydrogenation reaction enthalpy is calculated as *ca.* 48 kJ mol^{-1} H_2, which is far less than that of the pure $LiBH_4$ (*ca.* 74 kJ mol^{-1} H_2), demonstrating largely improved dehydrogenation thermodynamics of $LiBH_4$ through the doping of the Pt/G catalysts. Importantly, it should be noted that Pt nanoparticles supported on graphene play a crucial role in improving the hydrogen desorption and uptake reversibility of $LiBH_4$ at reduced temperature and pressure conditions. $LiBH_4$ is reformed and $Li_2B_{10}H_{10}$ is detected after being rehydrogenated at 400 °C for 10 h under 3 MPa hydrogen pressure, with a capacity of approximately 8.1 wt% in the 30th cycle. Thus, destabilizing $LiBH_4$ using the Pt/G catalysts is a new and promising way for the catalytic dehydrogenation and rehydrogenation of $LiBH_4$.

Acknowledgements

The authors gratefully acknowledge financial support from the National Science Foundation of China (21003015 and 21103014), the Science Foundation of Jiangsu Province (BK2012591, 12KJA150003, BE201113 and 2011Z0062), the Science Foundation of Changzhou (CJ20115020), the Foundation of Jiangsu Key Laboratory for Solar Cell Materials and Technology (201106), Jiangsu Key Laboratory for Green Catalytic Materials and Technology, Graduate Students Cultivation and Innovation project of Jiangsu Province (CXZZ12-0734), Qing Lan project of Jiangsu Province and the Priority Academic Program Development (PAPD) of Jiangsu Higher Education Institutions for support of this work.

References

1 C. Liang, Y. F. Liu, H. L. Fu, Y. F. Ding, M. X. Gao and H. G. Pan, *J. Alloys Compd.*, 2011, **509**, 7844.
2 Y. G. Yan, A. Remhof, S. J. Hwang, H. W. Li, P. Mauron, S. I. Orimo and A. Züttel, *Phys. Chem. Chem. Phys.*, 2012, **14**, 6514.
3 C. Wen, X. Zhang, S. E. Lofland, J. Lauterbach and J. Hattrick-Simpers, *Int. J. Hydrogen Energy*, DOI: 10.1016/j.ijhydene.2013.03.069.
4 I. Lindemann, A. Borgschulte, E. Callini, A. Züttel, L. Schultz and O. Gutfleisch, *Int. J. Hydrogen Energy*, 2013, **38**, 2790.
5 C. Wu, Y. Bai, J. H. Yang, F. Wu and F. Long, *Int. J. Hydrogen Energy*, 2012, **37**, 889.

6 C. C. Nwakwuo, T. Holm, R. V. Denys, W. Hu, J. P. Maehlen, J. K. Solberg and V. A. Yartys, *J. Alloys Compd.*, 2013, **555**, 201.
7 S. L. Lee, C. Y. Huang, Y. W. Chou, F. K. Hsu and J. L. Horng, *Intermetallics*, 2013, **34**, 122.
8 A. Etiemble, H. Idrissi and L. Roué, *Int. J. Hydrogen Energy*, 2013, **38**, 1136.
9 R. R. Shahi, A. P. Tiwari, M. A. Shaz and O. N. Srivastava, *Int. J. Hydrogen Energy*, 2013, **38**, 2778.
10 V. Knotek and D. Vojtěch, *Int. J. Hydrogen Energy*, 2013, **38**, 3030.
11 V. Tozzini and V. Pellegrini, *J. Phys. Chem. C*, 2011, **115**, 25523.
12 C. C. Huang, Y. H. Li, Y. W. Wang and C. H. Chen, *Int. J. Hydrogen Energy*, 2013, **38**, 3994.
13 C. Li, P. Peng, D. W. Zhou and L. Wan, *Int. J. Hydrogen Energy*, 2011, **36**, 14512.
14 A. Züttel, S. Rentsch, P. Fischer, P. Wenger, P. Sudan, P. Mauron and C. Emmenegger, *J. Alloys Compd.*, 2003, **356**, 515.
15 Y. F. Liu, H. Zhou, Y. F. Ding, M. X. Gao and H. G. Pan, *Funct. Mater. Lett.*, 2011, **4**, 395.
16 Y. F. Zhou, Y. F. Liu, W. Wu, Y. Zhang, M. X. Gao and H. G. Pan, *J. Phys. Chem. C*, 2012, **116**, 1588.
17 Y. F. Zhou, Y. F. Liu, Y. Zhang, M. X. Gao and H. G. Pan, *Dalton Trans.*, 2012, **41**, 10980.
18 J. H. Shim, Y. S. Lee, J. Y. Suh, W. Cho, S. S. Han and Y. W. Cho, *J. Alloys Compd.*, 2012, **510**, 9.
19 P. Ngene, M. H. W. Verkuijlen, Q. Zheng, J. Kragten, P. J. M. van Bentum, J. H. Bitter and P. E. de Jongh, *Faraday Discuss.*, 2011, **151**, 47.
20 J. E. Chen, Y. Zhang, Z. T. Xiong, G. T. Wu, H. L. Chu, T. He and P. Chen, *Int. J. Hydrogen Energy*, 2012, **37**, 12425.
21 J. F. Mao, Z. Guo, X. B. Yu and H. Liu, *J. Alloys Compd.*, 2011, **509**, 5012.
22 S. S. Deng, X. Z. Xiao, L. Y. Han, Y. Li, S. Q. Li, H. W. Ge, Q. D. Wang and L. X. Chen, *Int. J. Hydrogen Energy*, 2012, **37**, 6733.
23 M. R. Ghaani, M. Catti and A. Nale, *J. Phys. Chem. C*, 2012, **116**, 26694.
24 D. Blanchard, M. Zatti and T. Vegge, *J. Alloys Compd.*, 2013, **547**, 76.
25 R. X. Liu, D. Reed and D. Book, *J. Alloys Compd.*, 2012, **515**, 32.
26 J. Shao, X. Z. Xiao, L. X. Chen, X. L. Fan, S. Q. Li, H. W. Ge and Q. D. Wang, *J. Mater. Chem.*, 2012, **22**, 20764.
27 D. G. Liu, J. Yang, J. Ni and A. Drews, *J. Alloys Compd.*, 2012, **514**, 103.
28 K. Jiang, X. Z. Xiao, L. X. Chen, L. Y. Han, S. Q. Li, H. W. Ge and Q. D. Wang, *J. Alloys Compd.*, 2012, **539**, 103.
29 S. T. Sabitu and A. J. Goudy, *Int. J. Hydrogen Energy*, 2012, **37**, 12301.
30 H. P. Yuan, X. G. Zhang, Z. N. Li, J. H. Ye, X. M. Guo, S. M. Wang, X. P. Liu and L. J. Jiang, *Int. J. Hydrogen Energy*, 2011, **37**, 3292.
31 X. Y. Chen, W. Y. Cai, Y. H. Guo and X. B. Yu, *Int. J. Hydrogen Energy*, 2012, **37**, 5817.
32 X. B. Yu, Z. Wu, Q. R. Chen, Z. L. Li, B. C. Weng and T. S. Huang, *Appl. Phys. Lett.*, 2007, **90**, 1.
33 F. Agresti, A. Khandelwal, G. Capurso, S. L. Russo, A. Maddalena and G. Principi, *Nanotechnology*, 2010, **21**, 1.
34 B. C. Weng, Z. Wu, Z. L. Li, H. Yang and H. Y. Leng, *J. Power Sources*, 2011, **196**, 5095.
35 Z. Z. Fang, X. D. Kang, P. Wang and H. M. Cheng, *J. Phys. Chem. C*, 2008, **112**, 17023.
36 Y. Zhang, W. S. Zhang, A. Q. Wang, L. X. Sun, M. Q. Fan, H. L. Chu, J. C. Sun and T. Zhang, *Int. J. Hydrogen Energy*, 2007, **32**, 3976.
37 P. J. Wang, Z. Z. Fang, L. P. Ma, X. D. Kang and P. Wang, *Int. J. Hydrogen Energy*, 2010, **35**, 3072.
38 H. S. Lee, Y. S. Lee, J. Y. Suh, M. Kim, J. S. Yu and Y. W. Cho, *J. Phys. Chem. C*, 2011, **115**, 20027.
39 X. Liu, D. Peaslee, C. Z. Jost and E. H. Majzoub, *J. Phys. Chem. C*, 2010, **114**, 14036.
40 R. G. Utke, T. K. Nielsen, I. Saldan, D. Laipple, Y. Cerenius, T. R. Jensen, T. Klassen and M. Dornheim, *J. Phys. Chem. C*, 2011, **115**, 10903.
41 R. G. Utke, T. K. Nielsen, K. Pranzas, I. Saldan, C. Pistidda, F. Karimi, D. Laipple, J. Skibsted, T. R. Jensen, T. Klassen and M. Dornheim, *J. Phys. Chem. C*, 2012, **116**, 1526.
42 D. Colognesi, L. Ulivi, M. Zoppi, A. J. Ramirez-Cuesta, A. Orecchini, A. J. Karkamkar, E. G. Bardaji and Z. Zhao-Karger, *J. Alloys Compd.*, 2012, **538**, 91.
43 R. H. Scheicher, S. Li, C. M. Araujo, A. Blomqvist, R. Ahuja and P. Jena, *Nanotechnology*, 2011, **22**, 1.
44 J. Xu, R. R. Meng, J. Y. Cao, X. F. Gu, Z. Q. Qi, W. C. Wang and Z. D. Chen, *Int. J. Hydrogen Energy*, 2013, **38**, 2796.
45 P. Ngene, M. R. van Zwienen and P. E. de Jongh, *Chem. Commun.*, 2010, **46**, 8201.
46 J. Xu, X. B. Yu, Z. Zou, Z. L. Li, Z. Wu, D. L. Akins and H. Yang, *Chem. Commun.*, 2008, 5740.
47 Y. W. Zhu, S. Murali, M. D. Stoller, K. J. Ganesh, W. W. Cai, P. J. Ferreira, A. Pirkle, R. M. Wallace, K. A. Cychosz, M. Thommes, D. Su, E. A. Stach and R. S. Ruoff, *Science*, 2011, **332**, 1537.
48 X. L. Si, F. Li, L. X. Sun, F. Xu, S. S. Liu, J. Zhang, M. Zhu, L. Z. Ouyang, D. L. Sun and Y. L. Liu, *J. Phys. Chem. C*, 2011, **115**, 9780.
49 X. F. Liu, D. Peaslee, C. Z. Jost, T. F. Baumann and E. H. Majzoub, *Chem. Mater.*, 2011, **23**, 1331.
50 F. C. Gennari, *Int. J. Hydrogen Energy*, 2011, **36**, 15231.
51 J. J. Vajo, *Curr. Opin. Solid State Mater. Sci.*, 2011, **15**, 52.
52 P. Ngene, P. Adelhelm, A. M. Beale, K. P. de Jong and P. E. de Jongh, *J. Phys. Chem. C*, 2010, **114**, 6163.
53 Z. Z. Fang, P. Wang, T. E. Rufford, X. D. Kang, G. Q. Lu and H. M. Cheng, *Acta Mater.*, 2008, **56**, 6257.
54 J. Xu, X. B. Yu, J. Ni, Z. B. Zou, Z. L. Li and H. Yang, *Dalton Trans.*, 2009, 8386.
55 B. C. Weng, X. B. Yu, Z. Wu, Z. L. Li, T. S. Huang, N. X. Xu and J. Ni, *J. Alloys Compd.*, 2010, **503**, 345.
56 Y. J. Choi, J. Lu, H. Y. Sohn, Z. Z. Fang, C. Kim, R. C. Bowman Jr and S. J. Hwang, *J. Phys. Chem. C*, 2011, **115**, 6048.